The Electronic Structure of the Bacteriopheophytin *a* Anion Radical, in Vivo

Patrick J. O'Malley

Contribution from the Department of Chemistry, UMIST, Manchester, M60 1QD, U.K.

Received October 15, 1998. Revised Manuscript Received January 20, 1999

Abstract: Density functional calculations are used to calculate the electronic structure of the bacteriopheophytin *a* radical anion, $\phi_{A,}$ formed in the initial electron-transfer reactions of bacterial photosynthesis. Using the hybrid B3LYP functional together with the double ζ basis set EPR−II, ^{13}C, ^{1}H, ^{17}O, and ^{14}N isotropic and anisotropic hyperfine couplings are calculated and explained by reference to the electron density of the highest occupied molecular orbital and of the unpaired spin distribution around the radical. Good agreement is observed between calculated and experimental hyperfine couplings. Hydrogen bonding to the carbonyl group of ring E leads to minor changes in the unpaired spin density distribution and the resultant hyperfine couplings. The electronic structure of the anion radical form of the other bacteriopheophytin *a* molecule, ϕ_B, found along the inactive-electron-transfer (B) branch, is also studied, and the calculated electronic properties are compared with ϕ_A. It is shown that, whereas the electron density of the SOMO of the ϕ_A radical is delocalized along the acetyl group attached to the A ring, this delocalization is much reduced for the ϕ_B radical. The implication of this finding for selective electron transfer along the A branch is discussed.

Introduction

Initial electron transfer in the reaction center of *Rb sphaeroides* proceeds from the excited singlet state of the primary donor bacteriochlorophyll *a* molecule (D) to an acceptor B_A, a bacteriochlorophyll *a* molecule, in approximately 3 ps. After another 0.9 ps the electron is transferred to ϕ_A, a bacteriopheophytin *a* molecule, resulting in the formation of a bacteriochlorophyll *a* cation radical−bacteriopheophytin *a* anion radical ion pair.[1,2,3,4,5]

To obtain a quantitative understanding of these initial electron-transfer mechanisms one needs to know the spatial and electronic structure of the electron-transfer pigments involved. The well-resolved structures of the bacterial reaction centers of *Rps viridis*[6,7,8]and *Rb sphaeroides*[9,10,11,12] provide us with the spatial arrangement of the cofactors involved in electron transfer. The electronic structure of the pigments involved is not easily probed experimentally: EPR and ENDOR/TRIPLE resonance methods have been used to map the unpaired spin densities of the free radicals generated during the one-electron-transfer steps[13,14,15]. These methods predominantly use the proton hyperfine interaction terms to provide a map of the unpaired spin density distribution of the free radical involved, which, in turn, can be used to indirectly predict the electron density of the frontier orbitals(HOMO/LUMO) involved in the electron-transfer process. Proton hyperfine couplings provide an indirect probe of the electron density of the frontier orbitals, as spin density at the hydrogens arises usually from spin polarization or hyperconjugation with the main π electron system situated on the heavy atoms. There has been some, but somewhat sparse, success in obtaining ^{17}O, ^{15}N, or ^{14}N[16,17,18] hyperfine couplings for some biological free radicals. Unfortunately ^{13}C hyperfines, which would provide the best direct probe of the frontier orbital electron density, provide often insurmountable experimental problems and are rarely detected.

Accurate electronic structure prediction methods have been available for some time for small molecular systems. For the size of molecules encountered in photosynthetic electron transfer more approximate semiempirical methods have been principally employed. With suitable parametrization the INDO/SP method has been shown to provide good ^{1}H and ^{14}N isotropic hyperfine coupling prediction for chlorophyll- and pheophytin-type radicals.[19] Here, s spin populations are calculated which are then

(1) Okamura, M. Y.; Feher, G. *Annu. Rev. Biochem.* **1992**, *61*, 861.
(2) Deisenhofer, J.; Norris, J. R. *The Photosynthetic Reaction Centre*; Academic Press: San Diego, 1993.
(3) Blankenship, R. E.; Madigan, M. T.; Bauer, C. E. *Anoxygenic Photosynthetic Bacteria*; Kluwer Academic Publishers: Dordrecht, The Netherlands, 1995.
(4) Zinth, W.; Huppmann, P.; Arlt, T.; Wachtveitl, J. Philos. Trans. R. Soc. of London, Ser. A **1998**, *356*, 465.
(5) Feher, G.; Allen, J. P.; Okamura, M. Y.; Rees, D. C. *Nature* **1989**, *339*, 111.
(6) Deisenhofer, J.; Michel, H. *EMBO J.* **1989**, *8*, 2149.
(7) Deisenhofer, J.; Epp, O.; Miki, K.; Huber, R.; Michel, H. *Nature* **1985**, *318*, 618.
(8) Lancaster, C. R. D.; Michel, H. *Structure* **1997**, *5*, 1339.
(9) Yeates, T. O.; Komiya, H.; Chirino, A.; Rees, D. C.; Allen, J. P.; Feher, G. *Proc. Natl. Acad. Sci. U.S.A.* **1988**, *85*, 8487.
(10) Chang, C-H.; Tiede, D.; Tang, J.; Smith, U.; Norris, J.; Schiffer, M. *FEBS Lett.* **1986**, *205*, 82.
(11) Ermler, U.; Fritzsch, G.; Buchanan, S. K.; Michel, H. *Structure* **1994**, *2*, 925.
(12) Stowell, M. H. B.; McPhillips, T. M.; Rees, D. C.; Soltis, S. M.; Abresch, E.; Feher, G. *Science* **1997**, *276*, 812.
(13) Lendzian, F.; Huber, M.; Isaacson, R. A.; Endeward, B.; Plato, M.; Bonigk, B.; Mobius, K.; Lubitz, W.; Feher, G. *Biochim. Biophys. Acta* **1993**, *1183*, 139.
(14) Feher, G.; Isaacson, R. A.; Okamura, M. Y.; Lubitz, W.; *Biophys. J.* **1987**, *51*, 377a.
(15) Lubitz, W.; Isaacson, R. A.; Okamura, M. Y.; Abresch, E. C.; Plato, M.; Feher, G. *Biochim. Biophys. Acta.* **1989**, *977*, 227.
(16) Campbell, K. A.; Peloquin, J. M.; Diner, B. A.; Tang, X-S.; Chisholm, D. A.; Britt, R. D. *J. Am. Chem. Soc.* **1997**, *119*, 4787.
(17) Dole, F.; Diner, B. A.; Hoganson, C. W.; Babcock, G. T.; Britt, R. D. *J. Am. Chem. Soc.* **1997**, *119*, 11540.
(18) Kass, H.; Rautler, J.; Bonigk, B.; Hofer, P.; Lubitz, W. *J. Phys. Chem.* **1995**, *99*, 436.
(19) Plato, M.; Mobius, K.; Lubitz, W. In Chlorophylls. *CRC Handbook*; Scheer, H., Ed.; CRC Press: Boca Baton, FL, **1991**; pp 1015-1046.

10.1021/ja983630y CCC: $18.00
Published on Web 03/20/1999

converted to isotropic hyperfine couplings by multiplying by an empirically determined constant for each particular nucleus. As with all such methods the quality of the results depends on the choice of parameters and the well-known serious drawbacks of the INDO method[20] preclude its use as a general method in the study of free radicals. Chipman[20] has provided an excellent discussion of the limitations of the INDO method for electronic-structure calculations in general and for the calculation of hyperfine couplings in particular. The recent development of density functional methods, in particular so-called hybrid methods, now permits highly accurate wave functions to be obtained for large molecular systems. These methods have been particularly impressive in predicting properties of biological free radicals such as semiquinones, glycine, and tyrosyl.[21,22,23,24] Here, isotropic hyperfine couplings are rigorously obtained from a Fermi contact analysis, and anisotropic hyperfine couplings are obtained from the spin only electric field gradient at the nucleus. No empirical parameters are used in the hyperfine coupling calculation. The availability of such exact methods together with the availability of accurate coordinates for the electron-transfer pigments in bacterial photosynthesis permits us to calculate the electronic structure of such pigments and hence provide key insights on electronic pathways for electron transfer. As accurate hyperfine couplings, both isotropic and anisotropic, can be calculated with hybrid density functional methods, they also permit us to accurately assign experimentally determined hyperfine couplings to specific molecular positions. In such a fashion also, comparison between experimentally and theoretically determined hyperfine interactions can provide a test of the wave function calculated for the electron-transfer pigment.

Here we report on the electronic structure of the intermediate electron acceptor for the purple bacterial photosynthetic system, *Rb sphaeroides*, a bacteriopheophytin *a* molecule usually designated ϕ_A. The electronic structure of its anion-radical form is calculated using the B3LYP hybrid density functional method with a double ζ basis set, EPR−II;[23] spin-density distributions are calculated, and calculated anisotropic and isotropic hyperfine couplings are compared with experimental measurements. The effect of hydrogen bonding at the ring E carbonyl oxygen is also studied to investigate its effect on the electronic structure of the molecule. The electronic structure of the other bacteriopheophytin *a* found in the reaction center but not involved in electron transfer, ϕ_B, is also calculated and compared with ϕ_A.

Methods

The heavy-atom coordinates for ϕ_A and ϕ_B used for the calculations were obtained from the crystal-structure determination of *Rb sphaeroides* as determined by Erlmer et al.[11] and obtained from the Brookhaven database (1PCR). The crystal-structure coordinates correspond to the bacteriopheophytin *a* in the nonreduced state. Geometry optimizations performed in our laboratory on symmetrical models indicate only minor changes in geometry occur on reduction to the anion radical form. Hydrogens were added using standard bond lengths and angles. For computational purposes the ethyl group attached to ring B at C8 was truncated to a methyl group, and the long phytyl chain attached to ring D was similarly truncated to a methyl group, Figures 1and 2. Both are well removed from the main π electron system and will not affect the spin-density distribution of the free radical. The models used are shown in Figure 2. It has been shown that the OE1 atom of GluL 104 is within hydrogen-bonding distance of the O26 carbonyl oxygen atom of ϕ_A. We have modeled this hydrogen-bonding interaction by using the crystallographically determined positions for the GluL 104 oxygen and carbon atoms. The hydroxyl hydrogen was added using a standard bond length and angle and was placed such that all atoms making up the carboxylic acid group COOH were in the same plane. This gave an H−O26 hydrogen bond length of 1.7 Å. The remainder of the GluL 104 residue was truncated to a methyl group. This hydrogen bonded model, ϕ_A-HB is shown in Figure 2b.

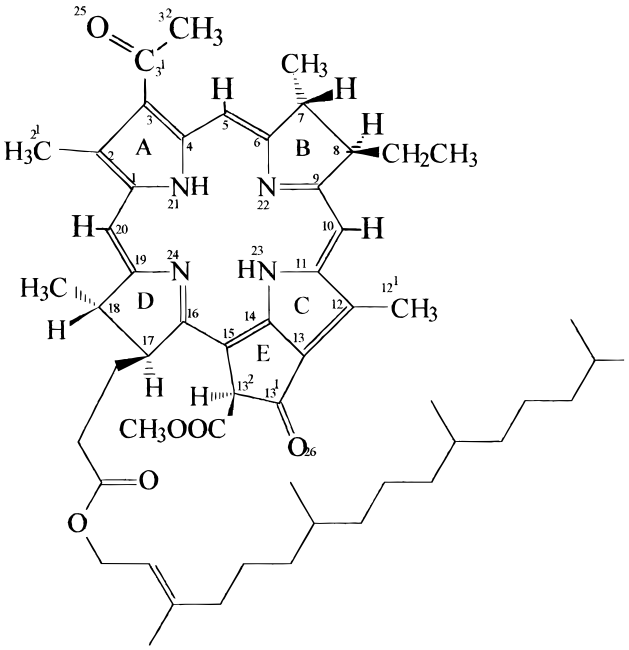

Figure 1. Molecular structure of bacteriopheophytin *a* together with numbering system used.

All density-functional calculations were performed using the Gaussian 94 electronic structure code.[25] The functional used was B3LYP. The basis set was EPR−II.[23] Graphical generation of electron-density surfaces was achieved using the SPARTAN package.[26]

Results and Discussion

ϕ_A. The SOMO (α HOMO) of the free pigment is shown in Figure 3 at three electron density contour values, (a) 0.09, (b) 0.07, and (c) 0.03 e/au^3. The tightest contour, Figure 3a, shows that the electron density of the HOMO is concentrated at the N22, N24, C2, C5, C10, C12, C15, C20, and O26 atom positions. More concentrated contours (not shown) demonstrate that the N22, N24, C12, and O26 positions have the highest concentration of electron density.

The intermediate 0.07 e/au^3, Figure 3b, contour shows that significant electron density is additionally found at O25, C1, C3, C13, and C13.[1] The diffuse contour at 0.03 e/au^3, Figure 3c, encompasses the majority of the electron density of the SOMO. Electron paramagnetic resonance methods, via the hyperfine interaction terms, measure the interaction of the magnetic nuclei with the unpaired spin density in the radical. While to a first approximation the unpaired spin density should

(20) Chipman, D. *Theor. Chim. Acta* **1992**, *82*, 93.
(21) (a) O'Malley, P. J.; Collins, S. J. *Chem. Phys. Lett.* **1996**, *259*, 296. (b) O'Malley, P. J. *Chem. Phys. Lett.* **1996**, *262*, 797.
(22) (a) O'Malley, P. J. *J. Phys. Chem. A* **1997**, *101*, 6334. (b) O'Malley, P. J. *J. Phys. Chem. A* **1997**, *101*, 6334. (c) O'Malley, P. J.; Ellson, D. A. *Biochim. Biophys. Acta* **1997**, *1320*, 65.
(23) (a) Barone, V. In *Recent Advances in Density Functional Methods*; D. P. Chong, Ed. World Scientific Publishing: Singapore 1995. (b) Rega, N.; Cossi, M.; Barone, V. *J. Amer. Chem. Soc.* **1998**, *120*, 5723.
(24) Himo, F.; Grasslund, A.; Eriksson, L. E. *Biophys. J.* **1997**, *72*, 1556.
(25) Frisch. M. J.; Trucks, G. W.; Schlegel, H. B.; Gill, P. W.; Johnson, B. G.; Wong, M. W.; Foresman, J. B.; Robb, M. A.; Head-Gordon, M.; Replogle, E. S.; Gomperts, R.; Andres, J. L.; Raghvachari, K.; Binkley, J. S.; Gonzalez, C.; Martin, R. L.; Fox, D. J.; Defrees, D. J.; Baker, J.; Stewart, J. J. P.; Pople, J. A. *GAUSSIAN 94*; Gaussian Inc.: Pittsburgh, PA, 1995.
(26) *SPARTAN 5.1*; Wavefunction Inc.: Irvine, California, 1997.

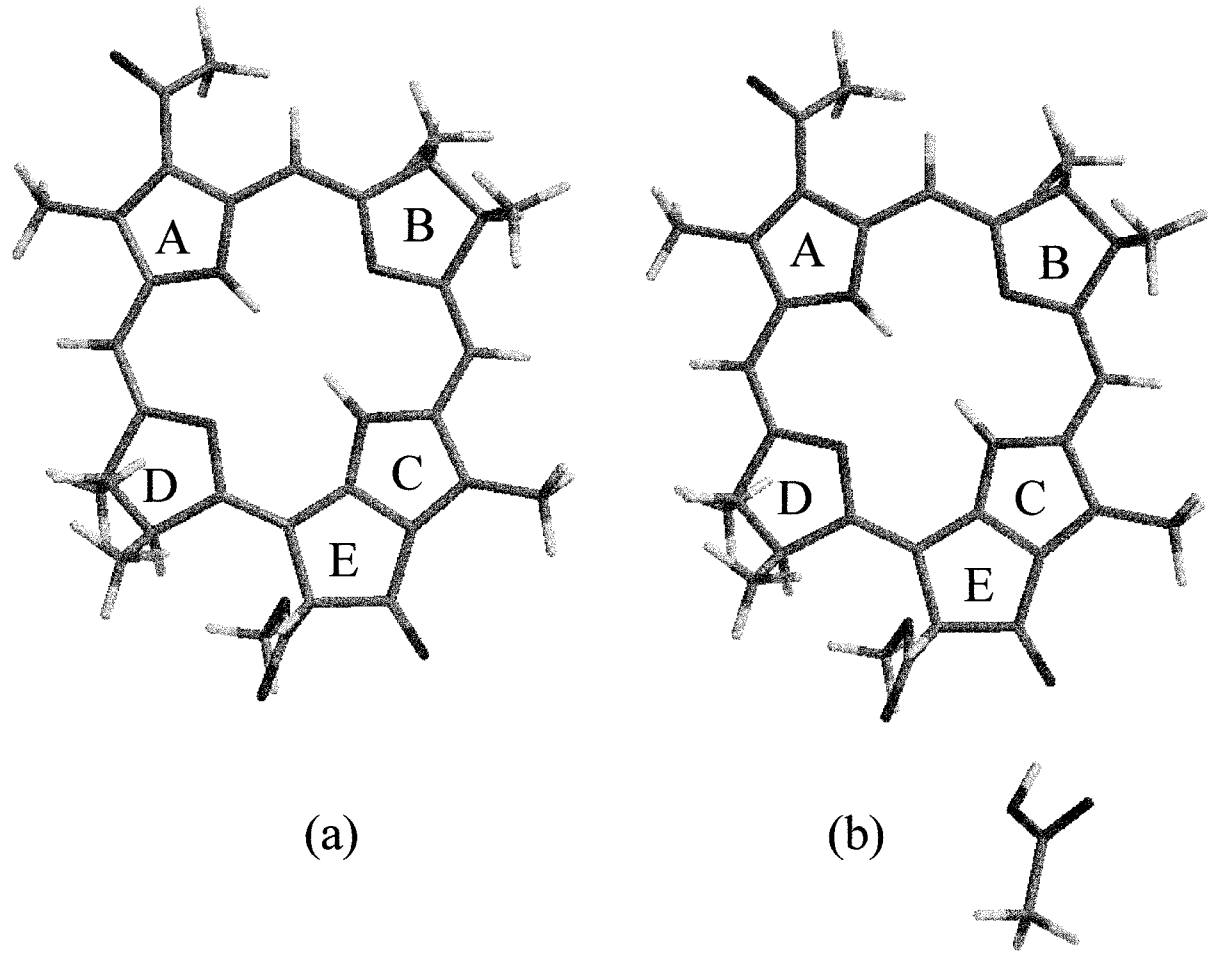

Figure 2. Models of (a) ϕ_A and (b) ϕ_A-HB used for the calculations. Heavy-atom coordinates are taken from the 1PCR Brookhaven database file. A similar model to ϕ_A was used for ϕ_B, again using the ϕ_B heavy-atom coordinates from 1PCR. The molecule orientation is as shown in Figure 1.

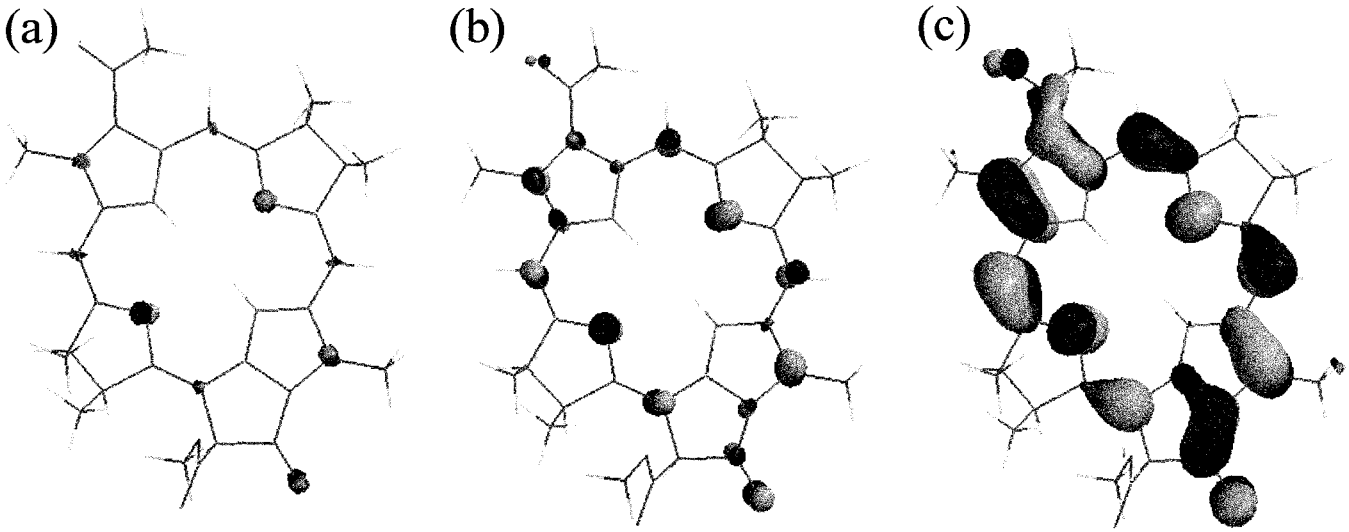

Figure 3. SOMO electron density contours for ϕ_A. (a) 0.09 e/au^3, (b) 0.07 e/au^3 and (c) 0.03 e/au^3. The molecule orientation is as shown in Figure 1.

correspond to the electron density of the SOMO, the exchange interaction between SOMO electrons and the other α electrons in the molecule gives rise to spin polarization which leads to regions of negative spin (excess β) within the radical. As can be seen from Figures 4a and b, the electron-density distributions of the SOMO are mirrored in the positive($\alpha-\beta$) unpaired spin density contours of Figure 4; high concentrations of positive spin density are found at N22, N24, C2, C5, C10, C12, C15, C20, and O26 with the highest concentration being found at N22, N24, and O26, Figure 4a. The negative (excess β) spin density plots of Figures 4c and d show how spin polarization leads to significant negative spin density at the N21, N23, C6, C9, C14, C13^2, C16, and C19 positions.

The anisotropic and isotropic hyperfine couplings calculated for the heavy-atom nuclei are presented in Tables 1−3. The anisotropic hyperfine couplings are a direct reflection of the

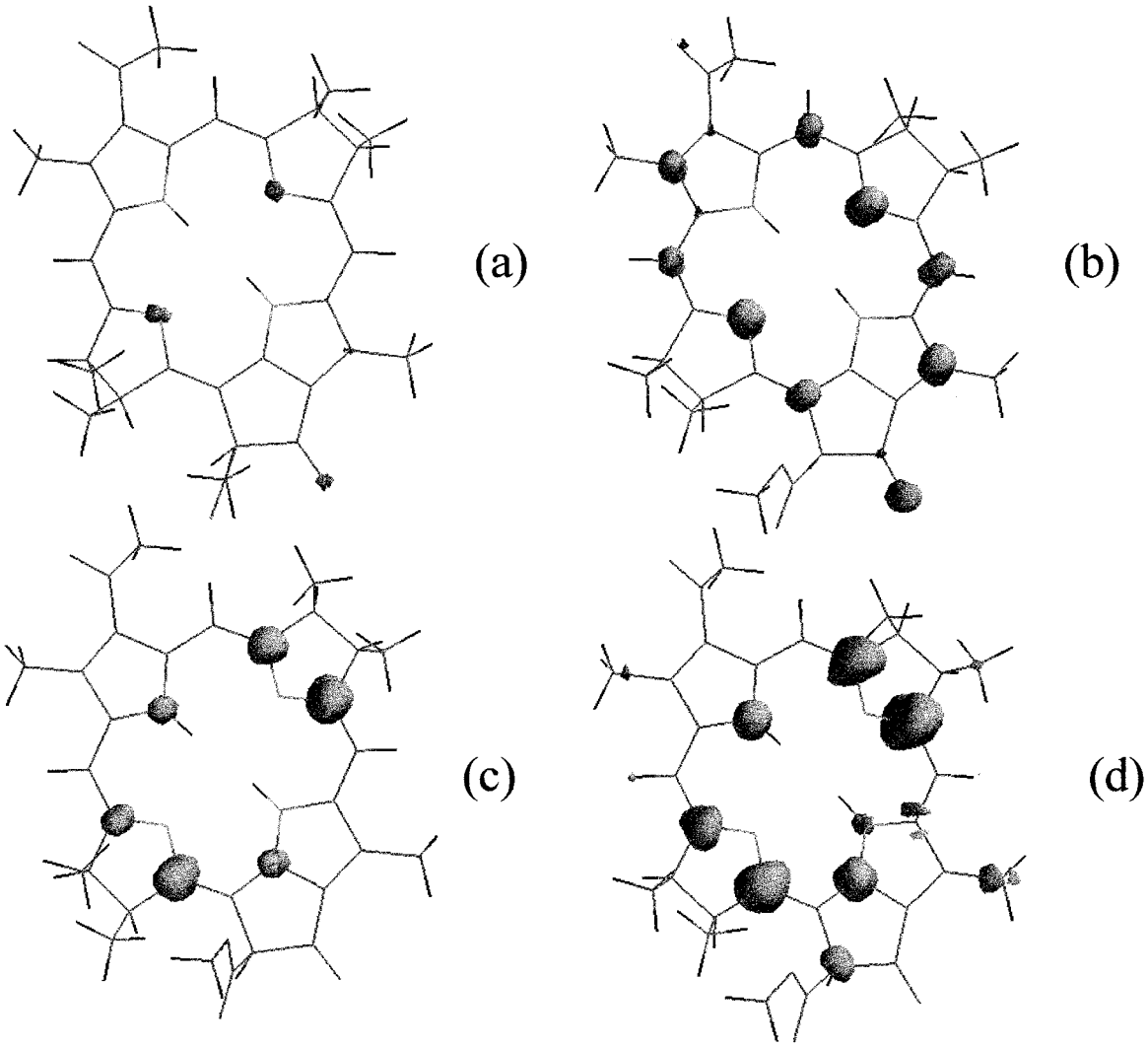

Figure 4. Unpaired spin density (α-β) contours for ϕ_A. (a)0.02 e/au^3, (b) 0.006 e/au^3, (c) -0.001 e/au^3, and (d) -0.0005 e/au^3. The molecule orientation is as shown in Figure 1.

spin-density plots of Figure 4. Large amplitude and axial tensors are observed for the high spin density positions N22, N24, and O26, Table 3. Large principal hyperfine tensor values are also found for positions C2, C12, and the methine positions C5, C10, C15, and C20, Tables 1 and 2. Interestingly, a major fraction of the unpaired spin is found at the O26 atom position of ring E. Relatively smaller magnitude principal hyperfine tensor values are found for the other atom positions which have small positive or negative spin densities.

The isotropic couplings arise from finite spin density at the nucleus concerned (Fermi contact interaction). In a π radical this spin density arises at the nucleus concerned via spin-polarization effects. The amount of spin at a particular nucleus will depend on the spin polarization created by the atom's own π spin density and also on neighboring-atom positions.[21] For the isotropic ^{13}C hyperfine coupling, π spin density at the atom itself will contribute positively, whereas π spin density on near-neighbor atoms contributes negatively. Hence, positions C2, C5, C10, C12, C15, and C20 have large positive ^{13}C isotropic couplings; C6, C9, C11, C14, C16, and C19 have negative values. Similarly, positive isotropic hyperfine couplings are found for N22 and N24 and negative values for O25 and O26 oxygen nuclei, as a result of the negative ^{17}O magnetic moment. In contrast, negative isotropic couplings are found for N21 and N23.

The calculated proton values in Table 4 reflect the spin density found at the neighboring carbon atoms. For H5, H10, and H20, which are bound to carbons having a high spin density, negative isotropic hyperfine couplings are found, reflecting the spin polarization from the nearby C5, C10, and C20 atoms which causes negative spin to arise at the hydrogen nuclei. The methyl-group hydrogens at C2 and C12 receive spin density predominantly via hyperconjugation of the hydrogens with the π-orbital lobe located at C2 and C12. Indeed, this hyperconjugation is in evidence in Figure 3c, where the conjugation of the SOMO on to the C12 methyl group hydrogens is shown. The methyl group is known to rotate freely even at cryogenic temperatures. The experimentally measured hyperfine coupling is therefore an average value over all orientations. To facilitate comparison with experimental determinations we have averaged the values for the three hydrogens of the methyl groups, and these are presented in Tables 4 and 5.

A proton ENDOR spectrum of the ϕ_A anion radical formed in *Rb sphaeroides* has been reported.[14] As a result of the complexity of the spectra and the absence of deuteration studies, no firm assignment of spectral lines to radical positions has been attempted. The four largest couplings observed in the experimental studies, at 11.0, 9.3, 8.7, and 7.5 MHz, were tentatively assigned to the methyl groups on rings A and C. These values are in quite good agreement with the calculated principal

Table 1. ^{13}C Isotropic (A_{iso}), and Anisotropic (T) Hyperfine Couplings Calculated for C1 to C10 (All Values Given in MHz)

atom	ϕ_A		ϕ_A−HB		ϕ_B	
	T_{11}		T_{11}		T_{11}	
	T_{22}	A_{iso}	T_{22}	A_{iso}	T_{22}	A_{iso}
	T_{33}		T_{33}		T_{33}	
C1	7.5	−1.3	8.4	−0.4	9.8	0.5
	−3.2		−3.7		−4.4	
	−4.3		−4.7		−5.4	
C2	15.8	5.6	14.9	4.9	13.3	3.7
	−7.8		−7.3		−6.6	
	−8.0		−7.6		−6.8	
C2[1]	0.4	−3.7	0.4	−3.5	0.4	−3.1
	−0.2		−0.2		−0.2	
	−0.2		−0.2		−0.2	
C3	8.3	1.5	8.5	1.8	11.0	1.8
	−4.0		−4.0		−5.3	
	−4.4		−4.4		−5.6	
C3[1]	2.6	−0.3	2.2	−0.7	0.9	−2.8
	−1.0		−0.8		−0.1	
	−1.6		−1.5		−0.8	
C4	3.0	−3.5	2.9	−3.6	6.3	−1.0
	−1.2		−1.2		−2.8	
	−1.8		−1.8		−3.5	
C5	16.2	9.6	16.3	9.7	16.1	7.8
	−8.0		−8.0		−8.0	
	−8.3		−8.3		−8.2	
C6	3.8	−12.6	3.7	−12.7	3.1	−11.5
	2.3		2.3		1.7	
	−6.1		−6.0		−4.8	
C7	0.3	0.7	0.3	0.6	0.3	0.2
	−0.1		−0.1		0.0	
	−0.3		−0.3		−0.3	
C8	0.4	1.4	0.4	1.6	0.3	0.8
	0.0		0.0		0.1	
	−0.4		−0.4		−0.3	
C9	5.3	−16.7	6.0	−17.8	4.5	−13.1
	3.9		4.6		2.9	
	−9.2		−10.6		−7.4	
C10	18.0	11.0	18.8	12.2	18.0	9.5
	−8.8		−9.2		−8.9	
	−9.2		−9.6		−9.2	

Table 2. ^{13}C Isotropic (A_{iso}) and Anisotropic (T) Hyperfine Couplings for C11 to C20 (All Values Given in MHz)

atom	ϕ_A		ϕ_A−HB		ϕ_B	
	T_{11}		T_{11}		T_{11}	
	T_{22}	A_{iso}	T_{22}	A_{iso}	T_{22}	A_{iso}
	T_{33}		T_{33}		T_{33}	
C11	0.8	−9.3	1.7	−11.7	1.5	−7.3
	0.2		0.6		−0.2	
	−1.0		−2.3		−1.3	
C12	24.6	12.9	27.9	15.4	21.8	10.1
	−12.1		−13.7		−10.7	
	−12.6		−14.2		−11.1	
C12[1]	0.3	−5.9	0.3	−6.5	0.4	−5.2
	−0.1		−0.1		−0.2	
	−0.2		−0.3		−0.2	
C13	5.9	−4.2	3.9	−7.0	5.9	−3.2
	−2.0		−0.8		−2.2	
	−3.8		−3.1		−3.7	
C13[1]	7.4	−0.2	12.8	3.3	6.0	−0.1
	−2.9		−5.8		−2.3	
	−4.5		−7.1		−3.8	
C13[2]	0.2	−4.9	0.3	−5.7	0.1	−3.9
	0.0		−0.1		0.0	
	−0.2		−0.2		−0.1	
C14	1.8	−4.4	2.3	−4.5	1.0	−3.9
	1.2		1.9		0.7	
	−3.1		−4.2		−1.7	
C15	17.3	9.5	16.5	9.5	16.9	9.9
	−8.4		−8.0		−8.3	
	−8.9		−8.5		−8.6	
C16	4.2	−11.2	4.6	−11.0	4.6	−12.0
	2.6		3.0		3.1	
	−6.9		−7.6		−7.8	
C17	0.3	1.1	0.3	1.2	0.2	1.0
	0.1		0.1		0.2	
	−0.4		−0.4		−0.4	
C18	0.2	−0.4	0.2	−0.6	0.3	−0.3
	0.0		0.0		0.0	
	−0.2		−0.2		−0.3	
C19	1.7	−7.9	1.0	−6.5	1.3	−7.8
	0.3		−0.3		−0.1	
	−1.9		−0.6		−1.2	
C20	14.6	4.7	13.1	3.6	14.3	4.6
	−7.1		−6.4		−7.0	
	−7.5		−6.8		−7.3	

Table 3. ^{17}O and ^{14}N Isotropic (A_{Iso}) and Anisotropic (T) Hyperfine Couplings (All Values Given in MHz)

atom	ϕ_A		ϕ_A−HB		ϕ_B	
	T_{11}		T_{11}		T_{11}	
	T_{22}	A_{iso}	T_{22}	A_{iso}	T_{22}	A_{iso}
	T_{33}		T_{33}		T_{33}	
N21	0.6	−1.4	0.6	−1.4	0.8	−1.9
	0.5		0.5		0.7	
	−1.1		−1.1		−1.5	
N22	12.6	6.8	12.5	6.9	13.2	6.7
	−6.2		−6.2		−6.5	
	−6.4		−6.3		−6.7	
N23	0.3	−0.3	0.2	0.1	0.3	−0.8
	0.2		0.1		0.3	
	−0.5		−0.3		−0.6	
N24	11.9	5.9	11.0	5.3	11.8	5.7
	−5.9		−5.4		−5.8	
	−6.0		−5.6		−6.0	
O26	−24.7	−5.9	−25.4	−6.7	−22.1	−5.3
	12.2		12.5		10.9	
	12.5		12.9		11.2	
O25	−7.5	−3.0	−7.2	−2.9	−3.6	−2.3
	3.7		3.5		1.7	
	3.8		3.7		1.9	

hyperfine tensor values for these two methyl groups presented in Table 4. For the bacteriopheophytin *a* anion radical in the solvent, dimethoxyethane, an extensive list of isotropic hyperfine couplings has been reported,[27] including the ^{14}N couplings. In Table 5 the isotropic hyperfine couplings calculated for our model are compared with the measured values. The agreement between theoretically predicted hyperfine couplings and experimental determinations is excellent and once more demonstrates the ability of hybrid density functional methods to provide quantitatively accurate hyperfine couplings. Moreover, such good agreement between experimental couplings and calculated values, without the aid of any parametrization, suggests that the wave function calculated is exact and the SOMO electron density plots in Figure 3 provide an accurate picture of the photoejected electron, approximately 4 ps after initial light excitation.

ϕ_A-HB. In the crystal structure determination of ref 11 the OE1 atom of GluL 104 was shown to be within hydrogen-bonding distance of the O26 oxygen of ϕ_A. As described in the Methods section we have taken the GluL104 heavy atom positions from the crystal-structure coordinates and added the hydrogen to the hydroxyl group. As described in the methods section the LGlu104 was truncated down to an ethanoic acid moiety. In Figure 5 the spin density, 0.007 e/au^3 contours, are compared for the hydrogen-bonded and non-hydrogen-bonded forms to investigate the change in spin density brought about by hydrogen-bond formation. The only discernible change in

(27) Lubitz, W.; Lendzian, F.; Mobius, K. *Chem. Phys. Lett.* **1981**, *84*, 33.

Table 4. ^{1}H Isotropic (A_{iso}) and Anisotropic (T) Calculated Hyperfine Coupling Constants (All Values Given in MHz)

atom	ϕ_A		ϕ_A−HB		ϕ_B	
	T_{11}		T_{11}		T_{11}	
	T_{22}	A_{iso}	T_{22}	A_{iso}	T_{22}	A_{iso}
	T_{33}		T_{33}		T_{33}	
H5	4.5	−7.0	4.5	−7.1	4.5	−7.1
	−0.9		−0.9		−0.8	
	−3.6		−3.7		−3.8	
H7	0.7	−2.0	0.7	−1.9	0.8	−1.9
	−0.2		−0.2		−0.2	
	−0.5		−0.5		−0.6	
H8	0.5	−3.0	0.4	−3.3	0.7	−2.4
	−0.1		0.0		−0.1	
	−0.5		−0.4		−0.6	
H10	4.7	−8.1	4.7	−8.5	4.8	−7.8
	−0.7		−0.6		−0.7	
	−4.0		−4.1		−4.1	
H13^2	1.1	−1.0	1.1	−0.1	1.1	−0.6
	0.2		0.2		0.4	
	−1.3		−1.4		−1.4	
H17	0.7	−2.3	0.6	−2.5	0.7	−2.7
	−0.1		0.0		0.0	
	−0.7		−0.6		−0.7	
H18	0.9	−1.1	1.0	−0.8	1.0	−0.9
	−0.2		−0.3		−0.3	
	−0.7		−0.7		−0.7	
H20	4.1	−5.8	3.8	−5.1	4.2	−6.1
	−0.9		−0.9		−0.9	
	−3.2		−2.8		−3.3	
H21	2.3	0.5	2.2	0.5	2.6	0.8
	−0.3		−0.3		−0.6	
	−2.0		−1.9		−2.1	
H23	2.0	0.0	1.7	−0.2	2.3	0.2
	0.0		0.2		−0.2	
	−2.0		−2.0		−2.1	
H(hb)			3.3	−0.1		
			−1.6			
			−1.7			
	A_{11}		A_{11}		A_{11}	
	A_{22}	A_{iso}	A_{22}	A_{iso}	A_{22}	A_{iso}
	A_{33}		A_{33}		A_{33}	
$CH_3(2^1)$[a]	8.0	6.5	7.7	6.2	6.6	5.1
	6.0		5.7		4.5	
	5.5		5.3		4.1	
$CH_3(12^1)$[a]	12.0	10.2	13.5	11.6	11.0	9.3
	9.7		11.0		8.8	
	9.1		10.4		8.2	

[a] For the methyl group protons at positions 2^1 and 12^1 the total (isotropic plus anisotropic) principal values (A) are given. These are obtained by averaging over the values calculated for a static orientation of the three hydrogens.

Table 5. Comparison of Isotropic Couplings Determined for the ϕ_A Anion Model and the Isotropic Hyperfine Couplings of the Bacteriopheophytin *a* Anion Radical Determined in Dimethoxyethane[27] (All Values Given in MHz)

position	calculated	experimental
N21	−1.4	−1.2
N22	6.8	7.2
N23	−0.3	−0.6
N24	5.9	6.2
H5	−7.0	−8.0, −8.5, −6.9
H10	−8.1	
H20	−5.8	
H7	−2.0	−1.5, −1.8, −2.6
H8	−3.0	
H17	−2.3	
H18	−1.1	
H12′	10.2	8.3
H2′	6.5	7.1

the spin density distribution is a noticeable increase at the $C13^1$ position. The isotropic and anisotropic hyperfine couplingscalculated on H-bond formation are shown in Tables 1−4. The most obvious change, brought about by hydrogen-bond formation, is an approximate doubling of the anisotropic tensor principal values for the $C13^1$ atom, mirroring the changes in spin density described above. Interestingly, little change is predicted to occur for the O26 atom position. The $C13^1$ increase in spin density is accompanied by a smaller decrease in the C13 atom tensor values. The hydrogen-bonded hydrogen atom of ϕ_A-HB has an anisotropic hyperfine coupling with the spin density of the bacteriopheophytin a anion dominated by the high spin density surrounding the O26 atom. The values calculated are given in Table 4. These correspond to total (anisotropic + isotropic) principal hyperfine tensor values of 3.2, −1.7, and −1.8 MHz. A hyperfine tensor having principal values of 1.92 and −0.93 MHz has been deduced from ENDOR spectroscopy on deuterium-exchanged samples and assigned to this proton interaction.[15] To reproduce these experimental values we have found it necessary to rotate the hydrogen of the hydrogen-bonding hydroxyl such the hydrogen bond distance (H−O26) is 2.1 Å. This is a quite long and unusual orientation for hydrogen bonding. As numerous other exchangeable ENDOR bands were found in the experimental study, it is not certain that the assigned bands do correspond to the GluL 104 hydrogen bond interaction. Specific deuteration of the GluL 104 hydroxyl hydrogen will be needed to resolve this uncertainty.

Electronic Structure Comparison of ϕ_A and ϕ_B. We have also performed a similar electronic structure study on the anion radical of the other bacteriopheophytin *a* found in the *Rb sphaeroides* reaction center, ϕ_B. ϕ_B is found on the inactive (B) branch for electron transfer and therefore is not reduced during the electron-transfer reactions of photosynthesis. It is of interest, however, to study the electronic properties of ϕ_B, particularly with a view to discerning any differences with ϕ_A which could account for the unidirectionality of electron transfer along the A branch in photosynthetic electron transfer. To this end, the electron density of the SOMO of the ϕ_B anion is compared with that of the ϕ_A anion in Figure 6. The SOMO electron density plots are very similar for most parts of the radical, but there is a discernible difference around the ring A, and particularly the acetyl group attached to ring A. For ϕ_A, the electron density of the SOMO is extended along the acetyl group; for ϕ_B, on the other hand, it is apparent that the delocalization of the SOMO on to the acetyl group is much reduced compared with ϕ_A. These SOMOs of the anion radicals correspond to the LUMOs of the unreduced bacteriopheophytins. The LUMOs of the pigments trace the pathway along which electron transfer occurs. According to the Marcus theory, electron transfer between two molecules depends on three principal factors:[5] the overlap of the electron densities, the difference in redox potential between the two molecules, and the reorganization energy. The maximum electron-transfer rate, for a given overlap, is predicted to occur when the reorganization energy equals the difference in redox energy, a situation which results in temperature independent electron transfer. Several of the electron-transfer reactions in photosynthesis satisfy this condition. According to Feher et al.,[5] electron-density overlap is the most crucial factor influencing rates of electron transfer between the cofactors of the bacterial photosynthetic reaction center, i.e., the electron transfer rate will be strongly influenced by electronic overlap between the LUMOs of the neighboring cofactors. The apparently greater extension of the LUMO for ϕ_A compared with that for ϕ_B may be a significant factor in the exclusive use of the A branch for electron transfer. In particular, it should be noted that the acetyl group of ϕ_A points directly at the bacteriochlorophyll *a* molecule,

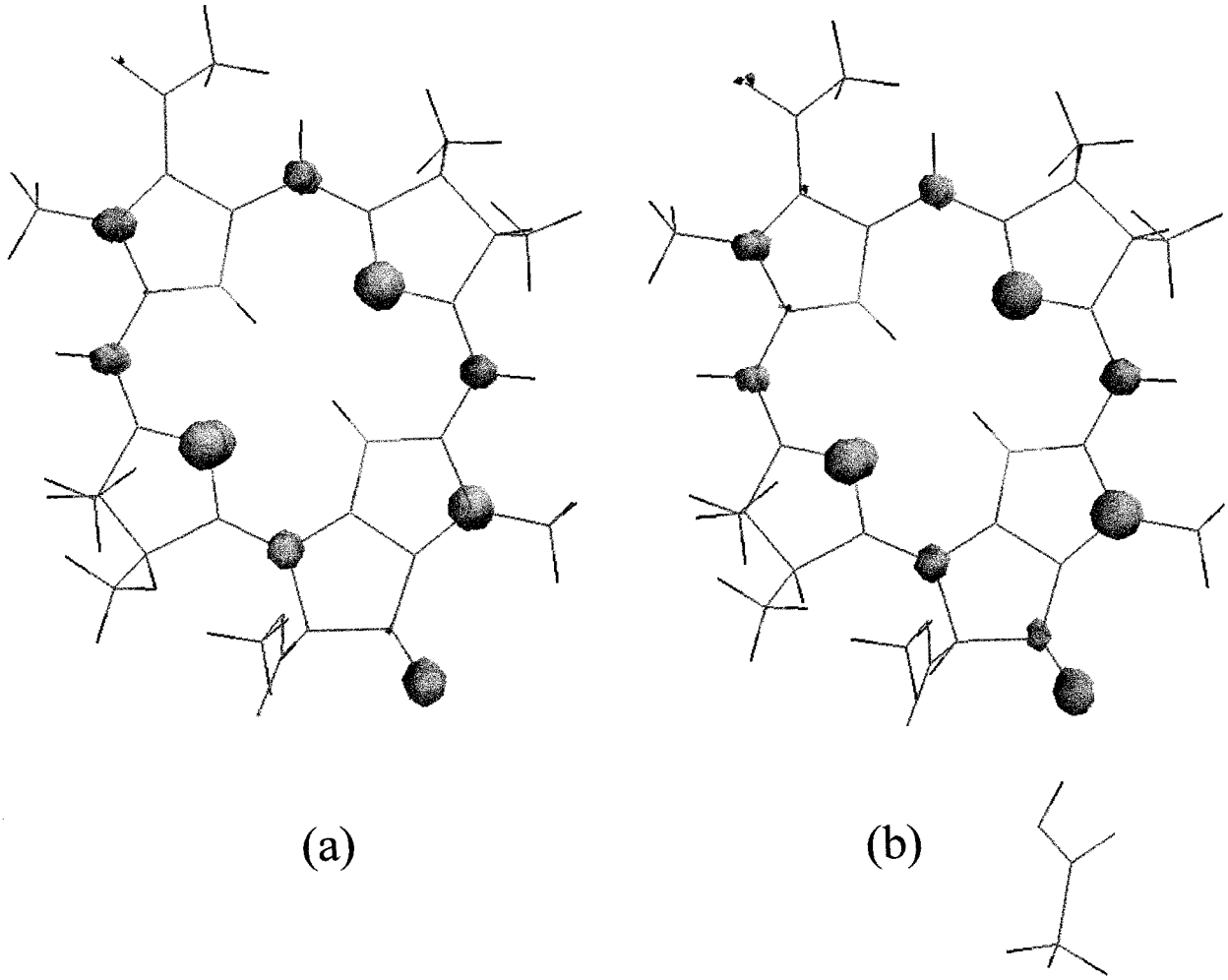

Figure 5. 0.007 e/au^3 unpaired spin density contours for (a) ϕ_A and (b) ϕ_A-HB. The molecule orientation is as shown in Figure 1.

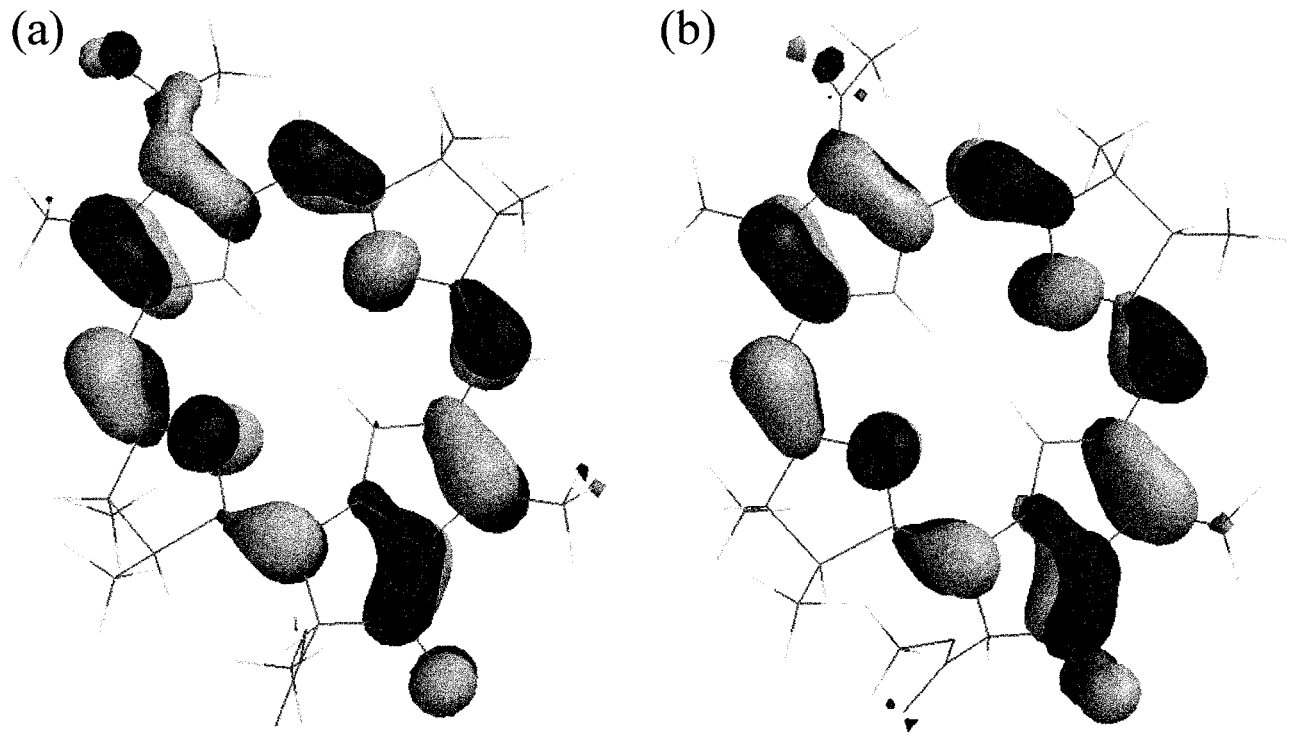

Figure 6. Comparison of SOMOS of ϕ (a) and ϕ (b). Contouring at 0.03 e/au^3. The molecule orientation is as shown in Figure 1.

B_A (see Figure 7) which precedes it in the electron-transfer chain.[11] The extension of the LUMO of ϕ_A readily extends the electronic pathway for electron transfer from B_A to ϕ_A. For the B branch ,the decreased extent of the LUMO on ϕ_B will lead

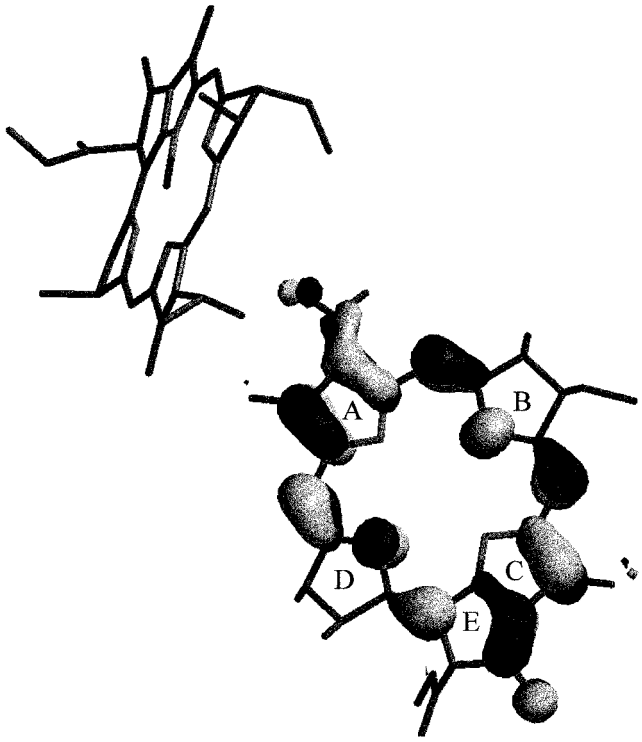

Figure 7. Orientation of the SOMO of the ϕ_A radical anion relative to the B_A molecule in the *Rb sphaeroides* reaction center, illustrating the extension of the SOMO of ϕ_A toward B_A. The coordinates are taken from the 1PCR file in the Brookhaven database.

to lower LUMO overlap between B_B and ϕ_B, thereby possibly inhibiting electron transfer.

The decreased delocalization onto the acetyl group for ϕ_B is caused by the larger dihedral angle that the acetyl-group plane makes with the main-ring plane for ϕ_B compared with ϕ_A. Greatest delocalization onto the acetyl group occurs when the acetyl plane is in the main-ring plane. As it is progressively moved out of the ring plane, by rotating the $C3C3^1$ bond, the delocalization of electron density onto the acetyl group is diminished. For ϕ_A, the $O25C3^1C3C2$ dihedral angle is 37°, whereas the corresponding dihedral for ϕ_B is 66°. A similar situation arises in the *Rps viridis* reaction center.[8]

The hyperfine couplings calculated for the ϕ_B anion radical are compared with the ϕ_A values in Tables 1−5. The principal differences between the two radicals occur for the ring-A and acetyl-group nuclei. For example the O25 and $C3^1$ anisotropic values are decreased in magnitude for ϕ_B as compared with those fir ϕ_A. This reflects the decreased spin density at these positions for ϕ_B due to the decreased delocalization of the SOMO onto the acetyl group. On the other hand, the magnitude of the C3 and C4 anisotropic tensor values are raised, reflecting the buildup in electron density at these positions for ϕ_B. Such changes will reverberate through the π-electron system, via spin polarization, leading to minor changes in hyperfine-coupling values throughout the radical.

Conclusions

The electronic structure of the bacteriopheophytin *a* anion radical forms of ϕ_A and ϕ_B in the reaction center of the photosynthetic bacterium *Rb sphaeroides* has been calculated using hybrid density functional methods. Calculated hyperfine couplings show good agreement with experimental determinations. Comparison of the electronic structures of ϕ_A and ϕ_B show major differences around ring A and its acetyl group. The greater extension of the frontier orbital onto the acetyl group for ϕ_A is proposed to promote good orbital overlap for electron transfer to occur.

JA983630Y